Acta Mech 216, 147–163 (2011)
DOI 10.1007/s00707-010-0361-2

M. D. de Tullio · G. Pedrizzetti · R. Verzicco

On the effect of aortic root geometry on the coronary entry-flow after a bileaflet mechanical heart valve implant: a numerical study

Received: 22 March 2010 / Revised: 1 June 2010 / Published online: 6 July 2010

Abstract The simultaneous replacement of a diseased aortic valve, aortic root and ascending aorta with a prosthesis is known as Bentall procedure (Bentall and De Bono in Thorax 23:338, 1968). This is a nowadays standard surgical approach in which the Valsalva sinuses of the aortic root are sacrificed and the coronary arteries are reconnected directly to the graft. The important function of the natural sinuses in the presence of the natural valve is well established; however, very little information is available about whether or not their presence can affect the functioning of a prosthetic bi-leaflet valve and the coronary flow. In the present work, we study the effect of the aortic root geometry on the blood flow through such devices, focusing the attention on the coronary entry-flow. Three root geometries have been considered, two mimicking the prostheses used in practice by surgeons (a straight tube, and the more recent tube with a circular pseudo-sinus), and a third maintaining the natural shape with three sinuses, obtained by Reul et al. (J Biomech 23:181–191, 1990) by averaging numerous angiographies of the aortic root in healthy patients. Direct numerical simulations of the flow inside the three prostheses, assumed as undeformable, under physiological pulsatile inflow conditions are presented. The dynamics of the valvular leaflets is obtained by a fully-coupled fluid–structure-interaction approach and the coronary perfusion is reproduced by modulating in time an equivalent porosity, an thus the resistance, of the coronary channels. The results indicate that the sinuses do not significantly influence the coronary entry flow, in agreement with the in vivo observations of De Paulis et al. (Eur J Cardio-thorac Surg 26:66–72, 2004). Nevertheless, the peak pressure at the joints of the coronary arteries is smaller in the *natural-like* aortic root geometry. The latter also produces a further beneficial effect of a reduction in the leaflets' angular velocity at the closure onto the valvular ring. These phenomena, if confirmed in more realistic clinical conditions, suggest that the use of a prothesis with physiologic sinuses would potentially reduce the local pressure peak, with the associated risk of post-operative bleeding and pseudo-aneurysm formation. It would also reduce the haemolysis effects caused by the red blood cells squashing between impacting solid artificial surfaces.

1 Introduction

The blood flow ejected from the left ventricle of the heart enters the aorta artery and, via the primary cardiovascular network, it distributes nutrients (i.e. oxygen) to the whole body. The aortic valve, located just

M. D. de Tullio
DIMeG and CEMeC, Politecnico di Bari, Via Re David 200, 70125 Bari, Italy

G. Pedrizzetti
DICA, Università di Trieste, P.le Europa 1, 34127 Trieste, Italy

R. Verzicco (✉)
DIM, Università di Roma "Tor Vergata", Via del Politecnico 1, 00133 Roma, Italy
E-mail: verzicco@imedado.poliba.it

downstream of the left ventricle, corresponds to the beginning of the aorta whose initial tract, the aortic root, shows a peculiar geometry: It is characterized by three sinuses (sinuses of Valsalva) where, from two of them, the coronary arteries originate. These small arteries have a great clinical relevance because they supply oxygenated blood to the myocardial muscle itself. Nowadays, the replacement of a diseased aortic valve with a mechanical or biological prosthesis enjoys a good acceptance in the clinical practice. In many cases, during the valve replacement procedure, the aortic root needs to be surgically reconstructed with a remodeling technique, or even sacrificed and replaced by a prosthesis with a re-implantation technique [3,7,11,12,27,41,49]. When, in particular, the disease affects simultaneously the aortic valve, the aortic root and the ascending aorta, the standard surgical approach is the Bentall [3] procedure, performed by implanting a polyethylene terephthalate fiber (Dacron) tube carrying a mechanical or biological valve. This routinely performed procedure provides a better annular stabilization combined with a superior support of the aortic wall. On the other hand, the root looses any extensibility at all levels [48], because of the material with different elastic characteristics (more rigid) with respect to the native aorta. Recently, a novel Dacron conduit that allows the reconstruction of pseudo-sinuses of Valsalva has been proposed by De Paulis et al. [13], even if this prosthesis does not reproduce three independent sinuses, but rather a single axisymmetric bulb.

A very delicate and important step following the remodeling or re-implantation of the aortic root involves the coronary arteries that supply the heart with oxygenated blood. In fact, the left and right coronary arteries, the very first two branches of the aorta, depart from the bottom of two of the Valsalva sinuses. An inability to supply adequate oxygenated blood to the heart muscle (ischaemia, myocardial infarction) is the cause of more morbidity and mortality in Western society than any other disease [35]. In surgery, the two coronaries, previously separated, need to be reconnected to the aortic root wall, as close as possible to their natural position. This procedure may have intra-operative (bleeding) and postoperative (bleeding and late pseudo-aneurysm formation) complications due to the high torsion or tension at the level of the coronary-root anastomoses: the introduction of valved Dacron conduits has simplified and expedited the surgical procedure, with reduced complications when compared with the remodeling technique [48]. The natural trilobed geometry of the aortic root is commonly associated to ensuring the proper opening of the natural aortic valve that has three leaflets opening to the wall in correspondence of the three sinuses. Very little information is available about whether or not this geometry can influence the dynamics of a prosthetic valve with two mechanical leaflets and consequently the coronary blood flow. Indeed, the nature of the coronary system is extremely complex, with branches that reach every part of the myocardium muscle forming a coronary network, variable among different individuals, that is one of the most compact and complex within the human body [51], difficult to access in vivo, and thus not completely known. Moreover, due to the difficulty in finding precise relationships between pressure and flow rate under different conditions, most of the contributions found in literature perform in vivo investigations. Kleine et al. [29] studied the influence of bi-leaflet and tilting disc valve orientation on coronary artery flow in pigs, finding that coronary blood flow was significantly influenced by the valve orientation and showing the optimum configuration for each valve model. De Paulis et al. [14] carried out an investigation of coronary flow after aortic root replacement in humans and they did not find any influence of pseudo-sinuses of Valsalva on the coronary flow reserve (later defined in Sect. 3.3). On the other hand, in the presence of sinuses or pseudo-sinuses they found a larger increase in the systolic component of coronary flow after maximal vasodilatation, which could indicate the role of sinuses or pseudo-sinuses in modulating the coronary flow pattern. While recently numerous numerical investigations on the flow through mechanical heart valves have been presented [5,6,10,15,22,34,36,43] considering both idealized and anatomic three-dimensional configurations, to our knowledge, the only previous numerical work present in literature including the geometry of the main coronary vessels is the work by Verhey and Bara [45] in which the effects on coronary flow produced by changes in the reinsertion technique are investigated. In particular, they studied how the variation of the outlet angle of the coronary arteries (modeled as tubes connected to the graft) could influence the coronary blood flow, by means of steady-state simulations of a laminar flow inside a straight tube, pseudo-sinuses and not carrying any valve. They found that the sinus design and variations of the outlet angle of the coronary arteries were able to minimally optimize the perfusion pressure and the velocities in the coronary circulation, although the changes in the different configurations were very limited and probably not yielding any clinical benefit.

In this work, we present a numerical investigation on the influence that the aortic root geometry has on the flow in the coronary arteries after a bi-leaflet mechanical heart valve implantation, under physiological conditions and considering several complete cardiac cycles. Three aortic root geometries have been used: a straight tube and a pseudo-sinuses-equipped tube (both mimicking the real prostheses used in surgery) and a channel with three anatomical sinuses (the *ideal* prosthesis), emulating as close as possible the natural geometry. The simplifying assumptions made to make this study feasible are the following: a) the geometries are considered

undeformable (since each prosthesis is anyway more rigid than the natural counterpart); b) the hinge mechanism of the leaflets is neglected (given its microscopic scale, it would require too high spatial resolution); c) the very complex as well as not clearly known coronary system is replaced by two channels departing from the aortic sinuses position and offering an equivalent resistance to flow; d) the fluid is considered as Newtonian (this is a safe assumption since the non-Newtonian nature of the blood manifests itself only in small vessels [35]).

High fidelity direct numerical simulations of the flow inside such complex and time-varying (due to the leaflets motion) geometries are carried out, resorting to a fluid–structure-interaction approach to describe the motion of the leaflets inside the fluid. We collect data from twenty cardiac cycles and present a comparison of several quantities for the three cases.

2 The problem

2.1 Flow field solution and fluid–structure interaction

Considering the sketch of Fig. 1, in every point of the time-dependent fluid domain $\Gamma + \Gamma_1 + \Gamma_2$ the Navier-Stokes equation for an incompressible viscous Newtonian fluid are solved :

$$\begin{aligned} \frac{\partial \mathbf{u}}{\partial t} + \nabla \cdot (\mathbf{uu}) &= -\nabla p + \frac{1}{Re}\nabla^2 \mathbf{u} + \mathbf{f} + \mathbf{f}', \\ \nabla \cdot \mathbf{u} &= 0, \quad \text{on} \quad \Gamma + \Gamma_1 + \Gamma_2 \end{aligned} \tag{1}$$

where $\mathbf{u}$ is the velocity vector, p is the pressure, $\mathbf{f}$ is the direct forcing of the immersed boundary method [16], $\mathbf{f}'$ is the forcing term for the coronary arteries described in Sect. 2.2 and Re is the Reynolds number later specified. The two leaflets B_1 and B_2 can rotate about their own pivots, and their angular displacements θ_i are governed by the following equations:

$$I_i \frac{\mathrm{d}^2\theta_i}{\mathrm{d}t^2} = T_i, \quad \text{for} \quad B_i \quad \text{with} \quad i = 1, 2, \tag{2}$$

where I_i are the dimensionless moments of inertia about the pivots and T_i are the tilting torques about the pivots resulting from the viscous stress tensor $\boldsymbol{\tau}$ and the pressure integrated over the leaflets surfaces S_i. Their specific expressions are

$$T_i = \int_{S_i} [(\boldsymbol{\tau} \cdot \mathbf{n} - p\mathbf{n}) \times \mathbf{r}] \cdot \hat{x} \mathrm{d}S, \tag{3}$$

with $\mathbf{n}$ the outer normal to the surface S_i of the i-th leaflet, $\mathbf{r}$ the vector given by the distance from the pivot axis to the surface element $\mathrm{d}S$ and $\hat{x}$ the unit vector aligned with the pivot axis. The incompressible Navier-Stokes

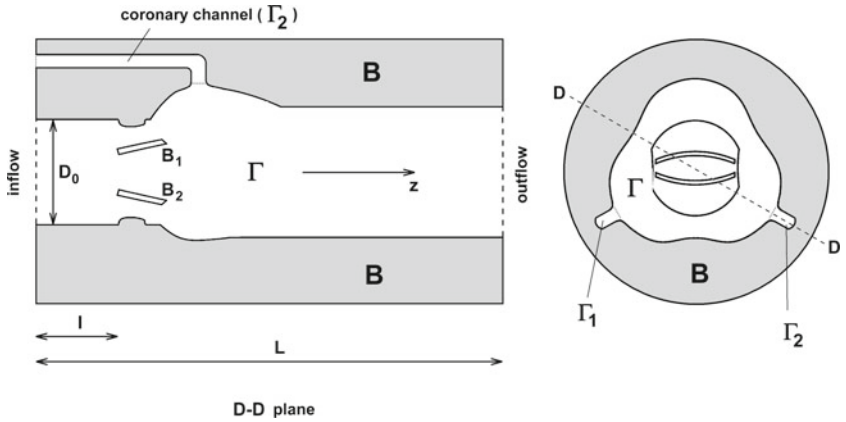

Fig. 1 Sketch of valve/root arrangement and computational domain ($L = 5D_0$; $l = D_0$)

equations are discretized in space using second-order-accurate central differences in conservative form and in cylindrical coordinates. The resulting system is inverted using a fractional-step method, where the viscous terms are computed implicitly and the convective terms explicitly. The large-banded matrix associated with the elliptic equation is reduced to a penta-diagonal matrix using trigonometric expansions (FFT's) in the azimuthal direction, and the resulting Helmholtz equations are then inverted using the FISHPACK package [44]. A third order Runge-Kutta scheme is used to advance the equations in time. All the simulations have been run with a fixed Courant number $CFL = 0.25$, thus having a variable time step Δt that is adjusted accordingly. Small time steps occur during opening and closing of the leaflets, thus allowing an accurate simulation of these phases, while larger time steps typically occur after valve closure, with a mean flow essentially zero and the leaflets still. More details on the Navier-Stokes solver are given in Verzicco and Orlandi [46], and Fadlun et al. [16]. The immersed boundary technique used in this work is the same as that used in a previous work [15], based on that proposed by Fadlun et al. and Iaccarino and Verzicco [16,24] and Cristallo and Verzicco [9]. A strong coupling scheme is employed for the solution of the system (1)–(2), since the prediction of the flow field and of the hydrodynamic loads requires the knowledge of the motion of the structure and vice-versa. A Hamming's 4th-order predictor—corrector method as described in Yang et al. [50] is used to integrate Eq. (2) through an iterative scheme until convergence is achieved. More in detail Eqs. (2) are expanded into a system of first order ordinary differential equations in the variables θ_i, $\dot{\theta}_i$, with the generalized loads L_i on the right hand side. The fluid and structural solvers are then coupled through an iterative scheme and, for each time step, the number of iterations l is determined by the condition $e_i = \mid \dot{\theta}_i^l - \dot{\theta}_i^{l-1} \mid < \epsilon$. In all our computations, a tolerance of $\epsilon = 10^{-4}$ was used and the number of iterations required for convergence at each time step varied from 1 to 4, depending on the phase of the dynamics; convergence is typically more difficult during the opening and closing phases when the leaflets rotate very rapidly while the criterion is satisfied already at the first iteration when the leaflets remain still or move slowly. In order to avoid numerical instabilities in the fluid–structure interaction algorithm induced by the added mass effect due to the very low moment of inertia of the valve leaflets [4], we employed an under-relaxation of the generalized loads according to $L_i = \gamma L_i^l + (1-\gamma) L_i^{l-1}$ with $\gamma = 0.9$, l the actual iteration level and $l-1$ the previous one. Further details on the method and several checks of the numerics can be found in de Tullio et al. [15].

2.2 Modeling coronary-entry-flow

The ultimate function of the coronary system is to deliver blood to the cardiac tissue, that is alternately contracting and relaxing. During systole, the contraction of the myocardium compresses the intra-myocardial capillaries, resulting in a *throttling* of these vessels. This effect ceases during diastole when the myocardium relaxes, and, although it is stretched by ventricular dilatation, the blood can better flow through the coronaries under the driving pressure gradient. This leads to a pulsatile flow in which the resistance cannot be simply related to the vessel radius. Even the geometrical formulation of the problem is very difficult due to the complex architecture of the coronary network: the precise branching structure of the system, one of the most compact and complex within the human body, could be mapped for each individual up to a limited level of details, most of the coronary small vasculature being deeply embedded within the cardiac muscular tissue [2,35]. Direct measurements of flow at the capillary output of the system are not possible, the precise number of capillaries (of the order of millions) being undeterminable as well as their flow velocity. On the other hand, some measurements are possible at the entry-level of the system, namely the left or right main coronary arteries departing from the aortic sinuses. In this work, we concentrate only on the very early vasculature of the coronary system, namely the two vessels connected to the Valsalva sinuses, assuming that everything downstream maintains the same behavior for different aortic geometries. Therefore, by *coronary blood flow* we indicate the flow through such main vessels, entering the coronary system, that is the only flow reasonably accessible for measurements. We have replaced the complex branching structure of the vascular system by two identical cylindrical rigid tubes connected to the coronary ostia of the aorta in the two sinuses of Valsalva (see Fig. 1). In this way, the entrance region of the coronary vessels is correctly modeled both in terms of diameter and position with respect to sinuses. The pressure gradient between the entrance region and the outflow of the tubes provides the driving force for the coronary flow. It is worth mentioning that two identical coronary arteries is the most common physiology, on average, however, it is just one among many possible physiological configurations that can be found, since there are cases in which the left artery feeds a much larger network than the right one (left dominance) or vice-versa (right dominance). In order to mimic the *tissue pressure effect* [26], that is the rhythmic contractions of the myocardium within each pumping cycle, a momentum loss for the points

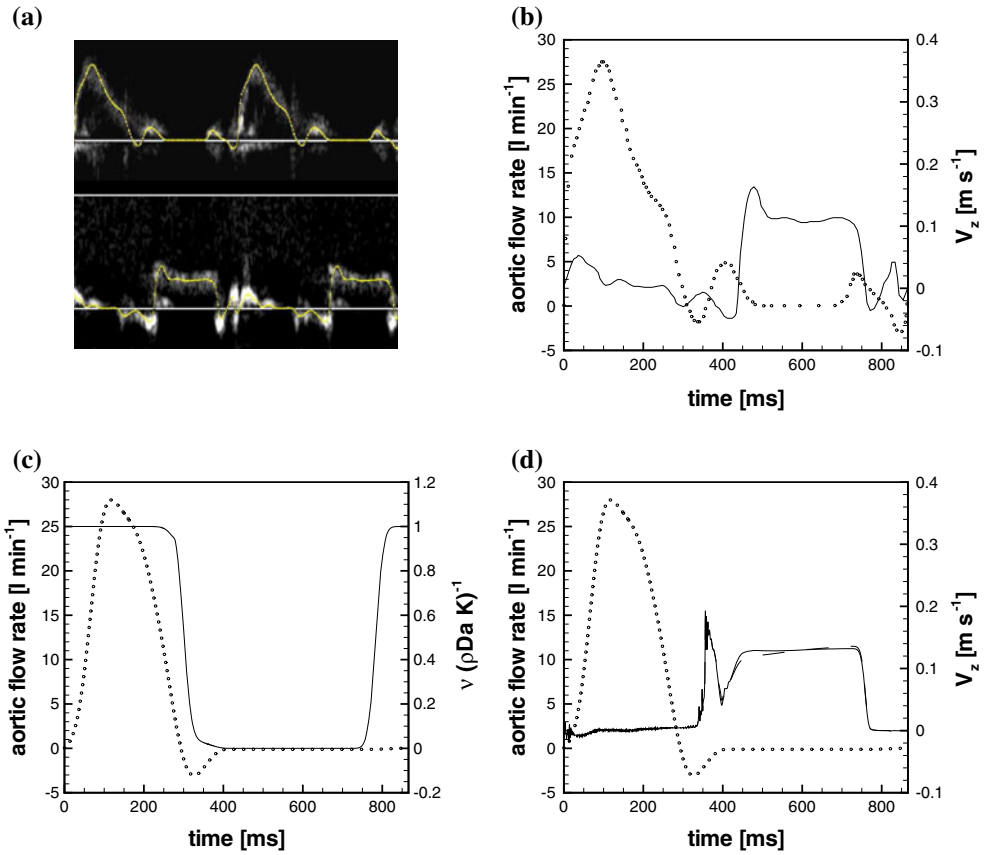

Fig. 2 **a** Aortic (*upper*) and coronaric (*lower*) velocity profiles by means of Pulse Wave Doppler echo-cardiography recorded in vivo in a young healthy man; **b** digitized aortic flow rate and mean coronaric velocity; **c** forcing term $\mathbf{f}'$ (4) inside coronaries in function of time; **d** computed average velocity in *left* (*continuous line*) and *right* (*dashed line*, almost invisible superimposed on the *continuous line*) coronary channel with diameter of $D_c = 6$ mm; the aortic flow (*dotted line*) is also reported for reference

inside the main coronary vessels tracts (Γ_1 and Γ_2) is provided, as done in a porous medium, by adding a time-variable extra forcing term in the Navier-Stokes equation:

$$\mathbf{f}' = \frac{\nu(\mathbf{u} - \mathbf{V_S})}{\rho Da K(t)}. \tag{4}$$

Here, $\mathbf{V_S}$ is the forced velocity inside the porous medium, $Da = K_0/L^2$ is the Darcy number, with K_0 and L a reference permeability and reference length, respectively, and $K(t)$ is a new free time-dependent parameter that modulates the porosity. If $K(t) \to \infty$ the forcing vanishes and the standard Navier-Stokes equations are recovered: this is set during diastole, when the fluid is allowed to flow through coronaries. If $K(t) \to 0$ the forcing becomes dominant in the equation yielding $\mathbf{u} = \mathbf{V_S}$: by imposing $\mathbf{V_S} = 0$ the no-flux condition inside the coronaries is obtained during systole. The effect of the forcing (4) on the system (1) is exactly known only for the extreme values of K, none of which can be used in a computational code. Accordingly, a *tuning* was necessary in order to modulate the forcing between these two extrema in such a way to obtain a realistic coronary flow rate. More in detail, the forcing was tuned so to reproduce, for the setup with the ideal aortic root and a coronary diameter $D_c = 6$ mm, a physiological flow similar to that observed by Pulsed Wave Doppler echo-cardiographic recording in a human being (Fig. 2a). The flow profile in this individual, a young man, has been chosen as it corresponds, by an expert cardiology judgment, to the most typically observed flow profile found in normal healthy conditions. In particular, the tuning was necessary at early diastole (negative peak of flowrate) in order to limit the high velocity peak that the suddenly reduced resistance of the channels provides: after 330 ms, the slope of the forcing curve is changed, maintaining the forcing larger than zero for about 70 ms (see Fig. 2c). It is worth noting that in practice the value of K cannot be ∞, therefore during systole the

Table 1 Geometrical parameters of the aortic root geometry shown in Fig. 3

$D_{B,\max}/D_0$	D_A/D_0	L_A/D_0	L_B/D_0	$r_{\max}/D_0$	$r_{\min}/D_0$
1.55	1.24	1.00	0.34	0.82	0.64

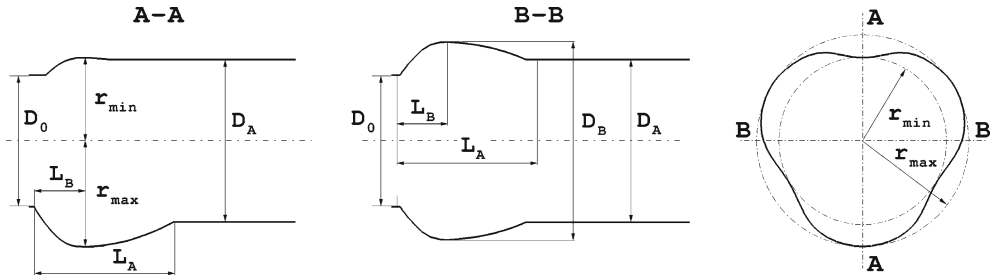

Fig. 3 Geometrical characterization of the aortic root with three sinuses of Valsalva [38]. Numerical values of the parameters are reported in Table 1

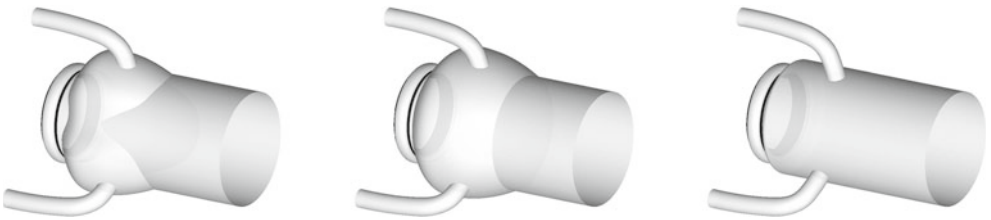

Fig. 4 Reproduced aortic root geometries and coronary channels with $D_c = 6$ mm used for calculations

computed coronary flow rate is not exactly zero. Once $\mathbf{f}'$ has been identified as in Fig. 2c it has been maintained identical in all other simulations in which the aortic root geometry or other flow details have been modified.

2.3 Aortic root and valve geometry

As discussed in the Sect. "Introduction", when the re-implantation technique is adopted in surgery, the diseased aortic wall is replaced with a Dacron conduit carrying a mechanical or biological valve. In the present study, we considered three models of aortic root. Two of them would mimic the available commercial prostheses: a standard straight tube and a conduit employing an axisymmetric bulb; the third prosthesis has been obtained following the study of Reul et al. [38], where numerous angiographies of the aortic root of patients without valve disease were evaluated and a *normal* geometry was derived, with the aim of mimicking as close as possible the three natural sinuses corresponding to the most common aortic root shape of healthy patients (note that, to the authors knowledge, there are no commercial prostheses with three sinuses available). The main geometrical parameters used for the characterization of the aortic root prostheses are the orifice diameter D_0 and the aortic diameter distal to the sinus D_A. Considering the three-sinuses prosthesis, the cross section in the sinus region can be approximately described by an epitrochoid (a curve, generated by a point which lies inside a circle which again rolls on the perimeter of the rolling circle), whose shape is a function of the ratio between the respective circle diameters. For this case, the diameters ratio of the inner and outer circles is 3:1, this means that we obtain three *lobes* with 120° spacing. The length of the sinus L_A, the maximum projected sinus diameter $D_{B,\max}$, and the distance between D_0 and $D_{B,\max}$, L_B along with other needed parameters are reported in Table 1.

The profile in Fig. 3 has been obtained using cubic splines through the given points, as done in Grigioni et al. [20]. Given the profile, for each z (Z being the axis directed in the flow direction) one can obtain the value of the projected diameter D_B and then can build an epitrochoid. In the regions close to the inlet and outlet boundaries, the epitrochoid could be inside the circles with diameters D_0 and D_A and then the section profile is composed of an epitrochoid truncated by the circles.

Finally, the axisymmetric prosthesis has been generated revolving around the Z axis the lower profile in the A–A plane in Fig. 3 (with $D_{B,\max} = 2r_{\max}$). A sketch of the three configurations is reported in Fig. 4.

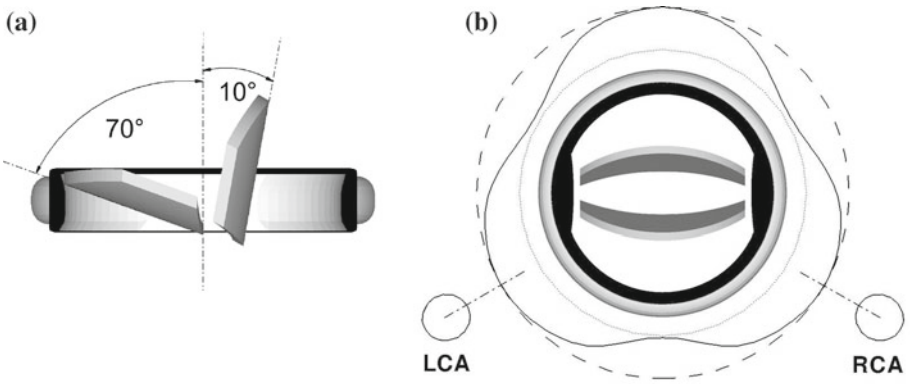

Fig. 5 **a** Range of rotation of the leaflets. **b** Positioning of the valve with respect to coronaries

Following de Tullio et al. [15], the valve model embedded in all the aortic roots reproduces the largely diffused bi-leaflet 27 mm Bicarbon prothesis by Sorin Biomedica [42]. The mounting scheme with respect to the sinuses and the two coronaries is reported in Fig. 5. In modeling the valve, the microscopic hinge mechanism has been neglected, while a small gap of about 340 μm (that is bigger than in the real prosthesis but is necessary to avoid computational problems when the valve is closed and ensure an adequate spatial resolution with 7 nodes across) in the hinge region has been left in order to allow the washing flow that occurs in the real mechanism. Finally, for all the cases, the friction at the hinges has been neglected. To avoid too high velocity values when the valve is closed, the leaflet range of rotation of 60° has been limited to 58° in the numerical simulations, leaving a few computational points through the area between the closed leaflet and the housing and between the two leaflets, that allow some back-flow (in other words, to avoid that the valve was apparently suddenly closed when no computational points where left in such gaps). Unlike de Tullio et al. [15] in this study the small axial leaflet translation, allowed by the complex hinge mechanism, has been neglected since it was not relevant to the aim of the present analysis.

2.4 Flow parameters and simulation details

We have assumed as main scaling quantities the inflow diameter $D_0 = 27$ mm and the bulk velocity at the peak inflow $U = 0.81$ m/s that with a blood kinematic viscosity $\nu = 3.04 \times 10^{-6}$ m^2/s yields a Reynolds number $Re = UD_0/\nu = 7{,}200$. The basic time unit is given by $D_0/U = 33.3$ ms so that, given the heart cycle of 866 ms, the Strouhal number is $St = D_0/UT \simeq 3.85 \times 10^{-2}$. The leaflets are made of pyrolytic carbon, with density of $\rho_l = 2{,}000\,\mathrm{kg/m^3}$, whereas the blood density is $\rho_b = 1{,}060\,\mathrm{kg/m^3}$. In dimensional units each leaflet has a rotational inertia of $7.947 \times 10^{-9}\,\mathrm{kg \cdot m^2}$ that when scaled with $\rho_b D_0^5$ becomes $I_i = 2.77 \times 10^{-4}$, $i = 1, 2$ used in Eq. (2).

The aortic root, the valve housing and the leaflets are discretized with unstructured triangular meshes (Stereo Lithography format, STL) and are embedded into the background cylindrical structured grid. In a previous work [15], at the same Reynolds numbers and in a similar configuration, three computational grids were tested in order to assess the grid independence of the results. It was found that the required resolution was achieved with a grid made of 193 × 137 × 250 nodes (about 6.6 millions points) in the azimuthal, radial and axial directions, respectively. In the present study, we use an even finer grid made of 217 × 165 × 250 nodes (about 8.95 millions points) in order to have enough grid points and accurately resolve the boundary layers in the tiny coronary channels. Within this mesh, the diameter of the coronary channels is discretized using about 35 grid nodes. The grid is uniform in the azimuthal and radial directions, while it is non-uniform in the axial direction and clustered near the valve, where rich vorticity dynamics is observed.

Twenty cardiac cycles are computed for all cases. Each cycle is discretized by a variable time step ranging, in dimensionless units D/U_0, from $\Delta t_{\min} = 10^{-4}$, (about 3 μs) occurring at the flow rate peak, to a maximum value of $\Delta t_{\max} = 7.5 \times 10^{-3}$, (about 250 μs) during the diastole. The CPU time for the computation of each complete cycle was equivalent to about 75 h on a single P-IV processor, equipped with 2 Gb of RAM.

The inflow velocity profile is assigned by an hyperbolic tangent function with stretching parameter $\gamma = 60$ which yields a flat velocity distribution in the bulk and accommodates the no-slip boundary condition at the aortic wall within a layer of thickness $\lambda/D_0 = 1/\sqrt{Re} \simeq 1.2 \times 10^{-2}$. This velocity profile is modulated in time to mimic the physiological flow rate produced by the heart in the left ventricle (Fig. 2) similarly to what already done by Romano [40] and de Tullio et al. [15]. The cycle duration was set at 866 ms, corresponding to about 70 beats/min (natural heart rate at rest). The mean flow rate was adjusted to about 5 l/min with a peak flow rate of about 28 l/min. These are typical physiological conditions under which an adult aortic valve operates.

3 Results

3.1 Basic flow features

In a previous work [15], a detailed numerical flow analysis for a configuration with three sinuses of the aortic root has been already carried out; readers are therefore referred therein for more details. In the following, we only summarize the key features of the flow and in particular we illustrate the differences produced by the three aortic root geometries. Figure 6 shows out-of-plane vorticity contours in the longitudinal plane containing one of the coronary channels (D–D plane of Fig. 1). The flow is sampled at four significant instants: (i) end opening of the leaflets; (ii) flow rate peak; (iii) start closure and (iv) end closure of the leaflets) clearly showing the small scale turbulence production from the instability of the shear layers released from the leaflets and valve housing.

Phase-averaged velocity profiles over twenty cardiac cycles have been computed, as well as maximum turbulent shear stress[1] and viscous stress[2] fields. Figures 7 and 8 report the profiles of these fields in the planes A–A and B–B (Fig. 3) downstream of the valve, corresponding to the nadir of curvature of the sinuses. The data are sampled at two instants of the cycle corresponding to the flow rate peak ($t \simeq 140$ ms) and to the beginning of the valvular closure ($t \simeq 220$ ms) in which the highest value of velocity and maximum turbulent stress levels are observed, respectively.

For the three configurations, during the opening phase the leaflets rotate synchronously, forming the three jets configuration typical of the bi-leaflet valves, with strong shear layers shed from the valve housing and the tips of the leaflets. At the peak of flow rate, about 25 ms after the leaflets reach the fully open position, the shear layers are unstable and a strong small-scale turbulence production is observed in the wake and in the sinuses region. Figures 7 and 8 show that the three velocity profiles are comparable in the three configurations, with some differences in the recirculation zone. Note that there is a recirculating region also for the case of the straight tube, since the valve orifice has a diameter smaller than the tube, and the flow experiences a small sudden expansion also in this case. The maxima turbulent shear stresses show peak values in correspondence of the leaflets wake and stagnation regions, while viscous stresses are stronger in correspondence of walls (leaflets and root), both showing comparable distributions in the three cases.

After the peak flow rate, when the flow starts decelerating, it is observed a transition to turbulence that generates small scale structures downstream the valve. The pressure gradient becomes increasingly adverse and the valve leaflets start closing at about 220 ms. At this time, although velocity values are ∼40% lower than at the flow rate peak, stresses maintain basically the same value and they are comparable for the three configurations. The valve closes completely at the negative flow peak ($t \simeq 325$ ms), and a leakage flow occurs from the hinge gaps and from the small gap between the leaflets and the valve housing. The turbulence level decreases and, in absence of any flow rate, the viscosity dissipates the small scale structures until the beginning of the new cycle.

These results reveal that the flow dynamics is highly dominated by the bi-leaflet configuration of the mechanical valve, that, given the presence of the two leaflets at the center of the orifice, forces the three-jets behavior and the vortex shedding. The aortic root geometry does not influence significantly the gross flow kinematics. Differently, a significant dynamic difference between the three geometries is shown by the pressure

[1] The maximum turbulent shear stress field is defined for each point by: $TSS^{3D}_{\max} = (\sigma_1 - \sigma_3)/2$, where σ_1 and σ_3 are the maximum and minimum principal shear stresses, obtained by the Reynolds stress tensor in the principal coordinate system and with a three-dimensional analysis [31,37].

[2] The reduction from the second–order viscous stress tensor to an equivalent scalar stress τ_{eq} has been performed according to the von Mises criterion used also by Apel et al. [1]. The expression of τ_{eq} is: $\tau_{\text{eq}} = \frac{1}{\sqrt{3}}\sqrt{\tau_{11}^2 + \tau_{22}^2 + \tau_{33}^2 - \tau_{11}\tau_{22} - \tau_{22}\tau_{33} - \tau_{11}\tau_{33} + 3(\tau_{12}^2 + \tau_{23}^2 + \tau_{13}^2)}$, where τ_{ij} are the viscous stress components.

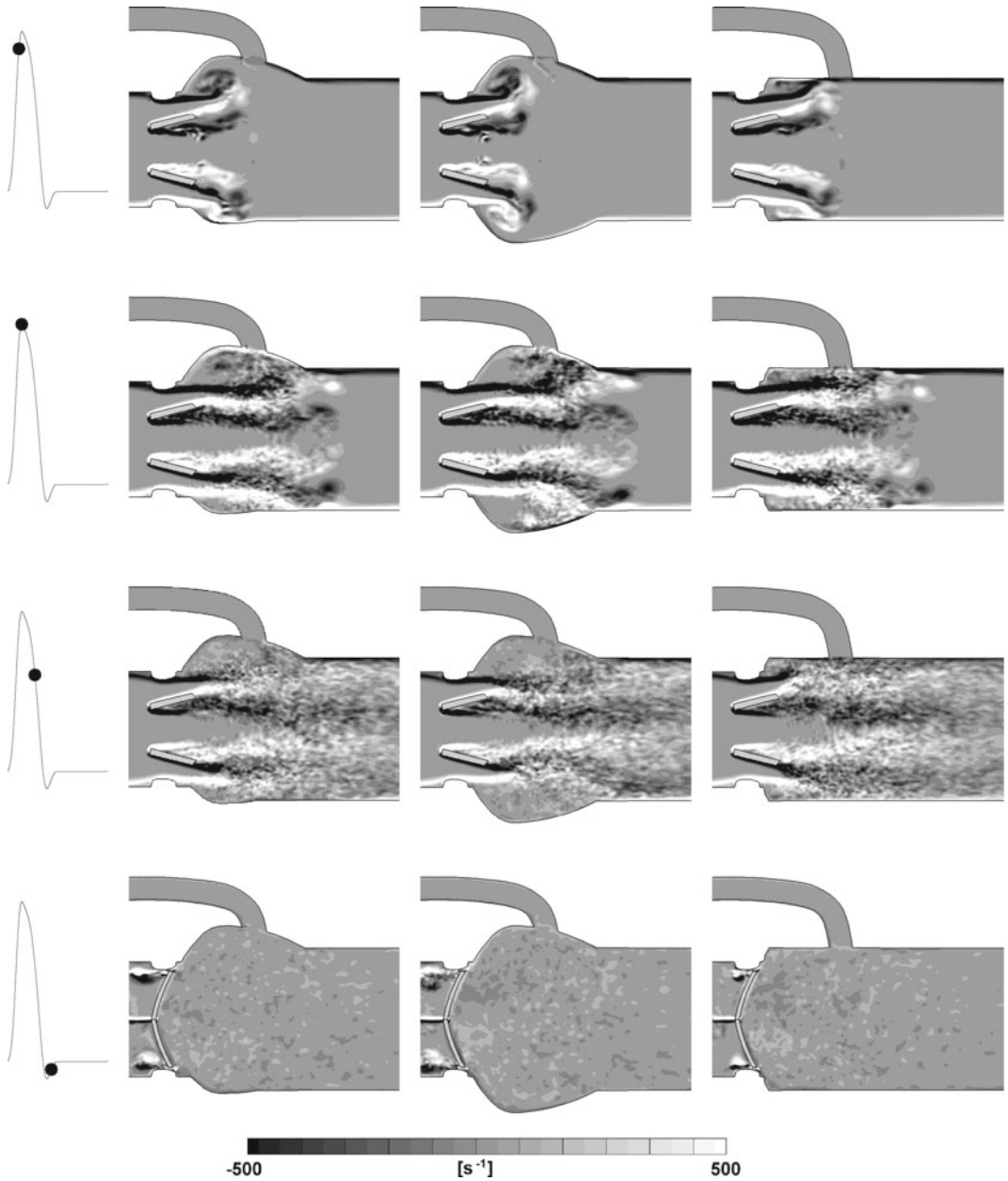

Fig. 6 Instantaneous out-of-plane vorticity contours in **D** − **D** plane at four significant instants (from *top* to *bottom*): end opening of the leaflets; flow rate peak; start closure; end closure of the leaflets

contours at the peak of flow rate (that is also close to the instant with maximum pressure), that is reported in Fig. 9, and the circumferential pressure distribution on the aortic root at the center of the coronary channel (Fig. 10). The geometry with three sinuses exhibits the lowest pressure values at the wall, while the straight pipe geometry presents the highest.

3.2 Leaflet dynamics

The phase-averaged leaflets angular positions for the three cases are shown in Fig. 11, together with the aortic flow rate for reference. The opening phase, occurring during the systole when the flow accelerates and prevents turbulence from developing, is directly driven by the incoming flow, it is well repeatable from cycle to cycle

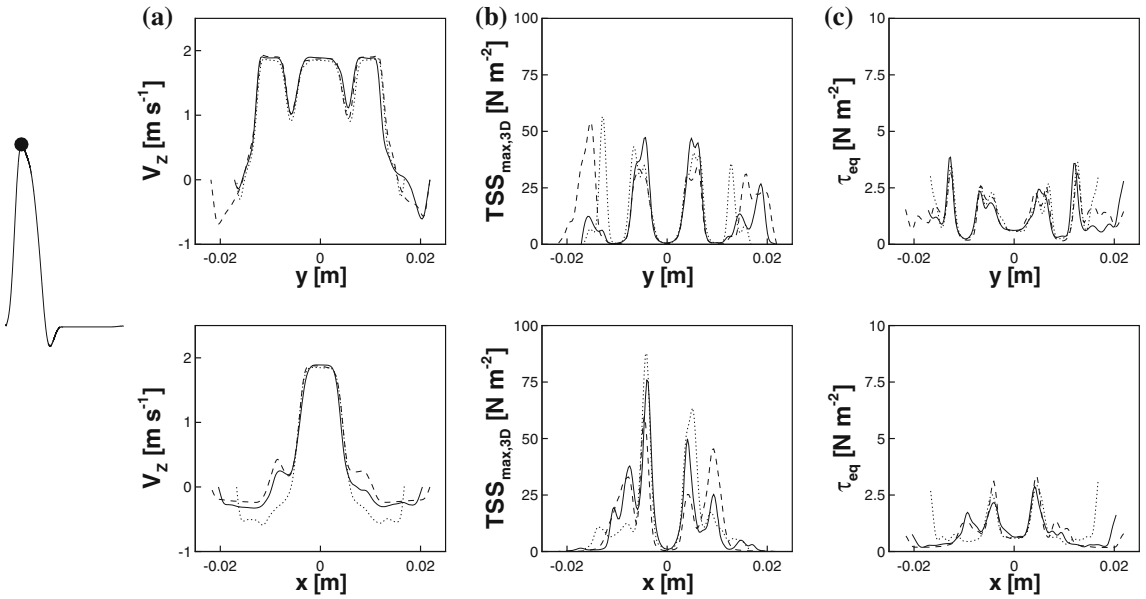

Fig. 7 Peak of flow rate: phase averaged streamwise velocity (**a**), maximum turbulent shear stress (**b**) and equivalent viscous stress (**c**) profiles in **A** − **A** (*upper*) and **B** − **B** (*lower*) planes in a section corresponding to the nadir of sinuses curvature. *solid line* three sinuses prosthesis; *dashed line* pseudosinuses prosthesis; *dotted line* straight tube prosthesis

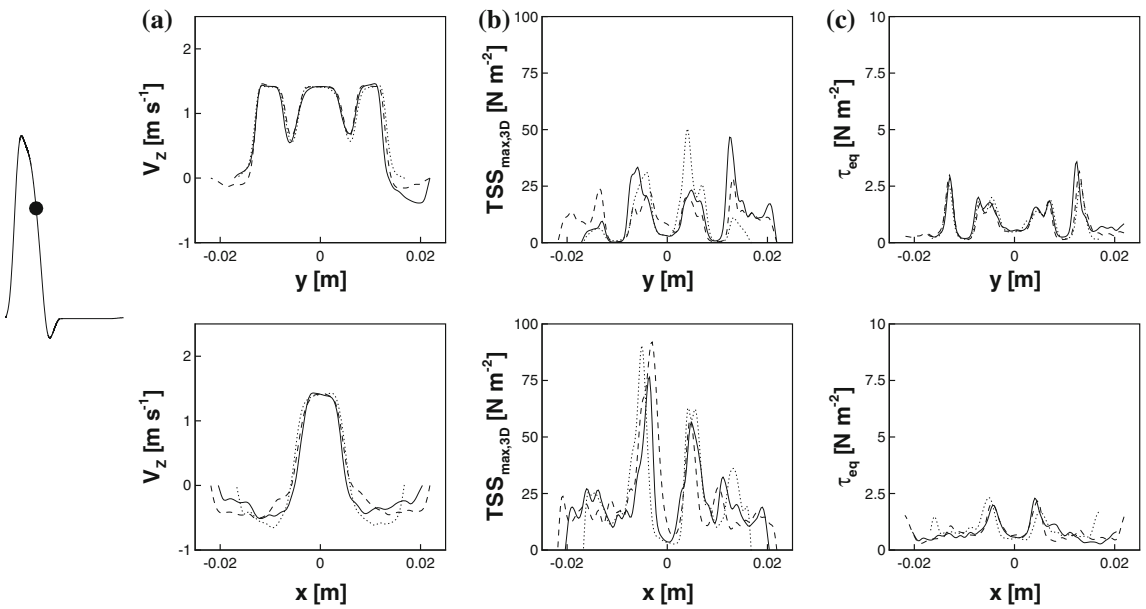

Fig. 8 Start of valvular closure: phase averaged streamwise velocity, (**a**) maximum turbulent shear stress (**b**) and equivalent viscous stress (**c**) profiles in **A** − **A** (*upper*) and **B** − **B** (*lower*) planes in a section corresponding to the nadir of sinuses curvature. *solid line* three sinuses prosthesis; *dashed line* pseudosinuses prosthesis; *dotted line* straight tube prosthesis

and shows little sensitivity to the aortic root geometry. Some differences arise during the leaflets closure, occurring during the deceleration of the flow, since the adverse pressure gradient promotes turbulence that, interacting with the leaflets and the root geometry, is responsible for high cycle to cycle variations, as well as slightly different dynamics for the three configurations. For the physiological aortic root the asynchronous closure of the leaflets, already observed by de Tullio et al. [15] and confirmed by the experiments of Romano [40], is induced by the asymmetric mounting scheme (5b) in which one of the leaflets faces the non-coronaric sinus of Valsalva while the other faces the junction of two sinuses. The closure delay between the two leaflets is of about 15 ms and it is observed at every cycle. Indeed, a small delay is observed also for the other two

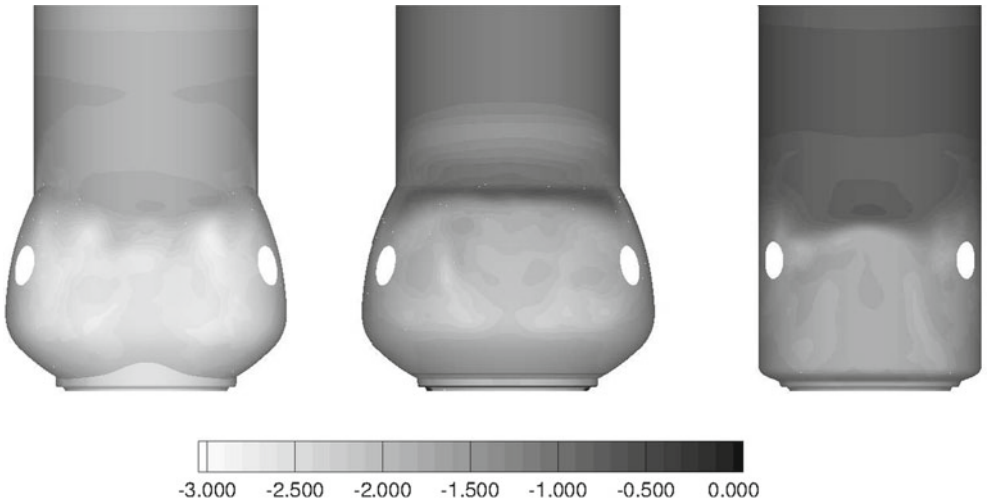

Fig. 9 Pressure distribution on the prosthesis walls at flow rate peak: $\frac{p-p_{\mathrm{ref}}}{\rho u_{\mathrm{ref}}^2}$, where p_{ref} is the left ventricular pressure

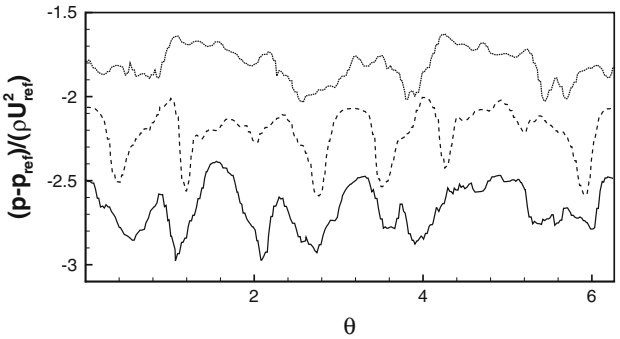

Fig. 10 Circumferential pressure distribution on the prosthesis walls at the center of coronary channel: $\frac{p-p_{\mathrm{ref}}}{\rho u_{\mathrm{ref}}^2}$, where p_{ref} is the left ventricular pressure

axisymmetric geometries, although it is limited to less than 5 ms and presents a strong variability from cycle to cycle; it would presumably disappear if the averages were made over a number of cycles much larger than 20. Figure 12 reports the phase-averaged angular velocity of the leaflets and it confirms that, apart from small oscillations, the dynamics of the valve is essentially the same for the three aortic roots. One significant difference occurs at the end of the valve closure ($t \simeq 350$ ms), when the leaflets hit the housing of the valve, an impact that occurs with a much smaller angular velocity (up to 250%) in the physiological aortic root with three sinuses.

3.3 Coronary flow

As already anticipated in Sect. 2.2 the coronary flow occurs mainly during the diastole when the ventricle dilates. The coronary flow rate is smaller during systole (although not negligible), increases abruptly after the valve closure, and then it remains constant up to the end of the cardiac cycle when it becomes zero again. The coronary flow rate is due to the pressure that develops at the sinuses, and Fig. 13 shows the pressure distribution at 366 ms, when the maximum coronary flow rate occurs; this pressure difference is about 15 mmHg showing only small variations for the three configurations. Figure 14a shows the computed total coronary blood flow for the case of channels with diameter of 6 mm, and the mean values of the coronary flow are reported in Table 2. All the configurations provide essentially the same flow rate, since the aortic root with three sinuses yields the highest mean flow-rate but the maximum difference is of the order of 5.0%.

In this configuration, the computed mean coronary flow (little below 200 ml/s) is close to the upper level of the physiological flow range, that can be up to about 5% of the aortic flow [17], that for our setup is

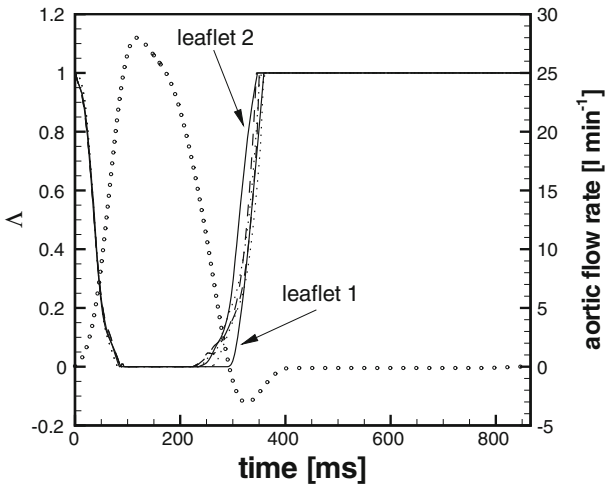

Fig. 11 Time variation of the phase-averaged leaflets angular position $\Lambda = \frac{(\alpha_{\text{open}} - \alpha)}{(\alpha_{\text{open}} - \alpha_{\text{closed}})}$ (*solid line* three sinuses prosthesis; *dashed line* pseudosinuses prosthesis; *dotted line* straight tube prosthesis) and aortic flow rate (*open circle*)

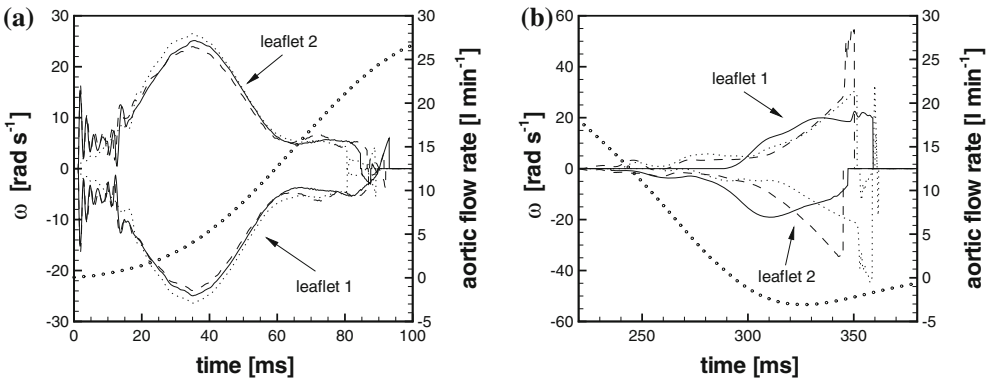

Fig. 12 Time variation of the phase-averaged leaflets angular velocity (*solid line* three sinuses prosthesis; *dashed line* pseudosinuses prosthesis; *dotted line* straight tube prosthesis) and aortic flow rate (*open circle*). **a** opening phase; **b** closing phase

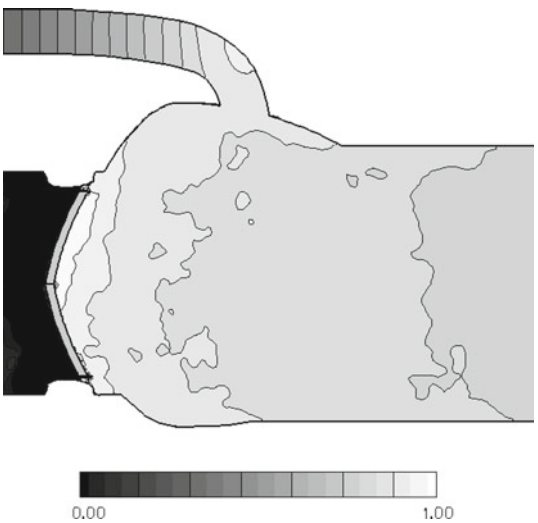

Fig. 13 Pressure distribution in the **D** − **D** plane after valve closure for the three sinuses prosthesis: $\frac{p - p_{\text{ref}}}{\rho u_{\text{ref}}^2}$, where p_{ref} is the left ventricular pressure

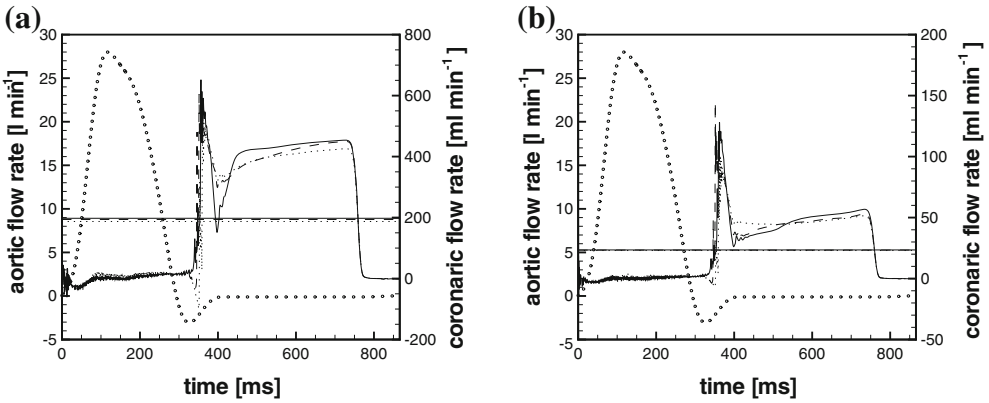

Fig. 14 Time variation of the phase-averaged total coronaric flow rate (*solid line* three sinuses prosthesis; *dashed line* pseudo-sinuses prosthesis; *dotted line* straight tube prosthesis) and aortic flow rate (*open circle*). **a** coronary channels with $D_c = 6$ mm; **b** coronary channels with $D_c = 3$ mm

Table 2 Computed mean total coronaric flow rate (in ml/min) for the three configurations with different coronaric diameters

	Valsalva	Axisymmetric	Channel
$D_c = 6$ mm	197.6	193.8	187.21
$D_c = 3$ mm	23.47	23.32	22.99
$D_c = 3$ mm; anticipated case	124.2	125.4	107.7

about 250 ml/min. The coronary arteries supply the heart with oxygenated blood and the oxygen demand, and coronary discharge as well, cover a wide range passing from resting to maximal activity conditions. In the latter, (because of e.g. physical exercise, reactive hyperemia, or drug infusion) the coronary blood flow can increase up to six times resting values. On the opposite, during a prolonged rest state a significant decrease of the coronary flow rate is obtained (after parasympathetic activation) by the increase of coronary vascular resistance due to the constriction of the vessels [47], since the driving pressure gradient is allowed to change by a relatively small amount (of the order of some ten percent). The difference between coronary blood flow at the peak of vasodilatation and basal flow is known as *coronary flow reserve*. In our numerical model, the resting condition is simulated by halving the coronary diameter, while the previously simulated cases are taken as a reference high activity state (stress state). Figure 14b and Table 2 show the total coronary blood flow in this case. Again, no relevant differences are found between the three configurations, thus confirming the results obtained so far; with a small increase (within 2%) in the case of three Valsalva sinuses. As expected, a significant difference in the coronary flow is not found. Several authors [33,39] proposed the concept that within the cardiovascular system the diameters of the main arteries are related to the flow rate the vessel has to convey. Known as the *cube law* it states the proportionality of the flow rate through a vessel to the cube of vessel diameter, and it continues to have a wide support in terms of biological data [23,33,39,51,52]. The ratio between the two mean flow rates q_1/q_2 is 8.4, 8.3 and 8.1 for the three sinuses, the pseudo-sinuses and the straight channel prosthesis, respectively, and it is reasonably close to the cube law value of 8.

Before concluding this section, we wish to stress that in this study the time variation of the coronaric flow rate was determined by the forcing described in Sect. 2.2 that, in turn, was tuned in such a way to replicate a specific human echo-cardiographic image (Fig. 2a). This case, however, although quite general, is not representative of all possible situations that show a flow also in the systolic phase, a non constant (decreasing) flow rate during the diastole and many other minor features. In order to verify whether our previous conclusions are sensitive to changes in the flow rate time profile, we have performed another set of simulations in which the coronary resistance due to porosity reaches the zero value already during the deceleration phase, when the valve is still open (Fig. 15a). As shown by Fig. 15b also in this case the coronary flow rate shows basically the same behavior for the three aortic roots, although either the mean flow rate (Table 2) and its instantaneous time evolution are different from Fig. 14b. The main noticeable difference is a reduction of the mean flow rate of about 14% for the case of the straight channel while the geometries with the axisymmetric bulbous and the three Valsalva sinuses provide the same flow rate. These results are in agreement with the in vivo study of De Paulis et al. [14]. The authors indicate that the presence of sinuses or pseudo-sinuses does not influence the coronary flow reserve. However, they have also found a greater increase in the systolic component of coronary

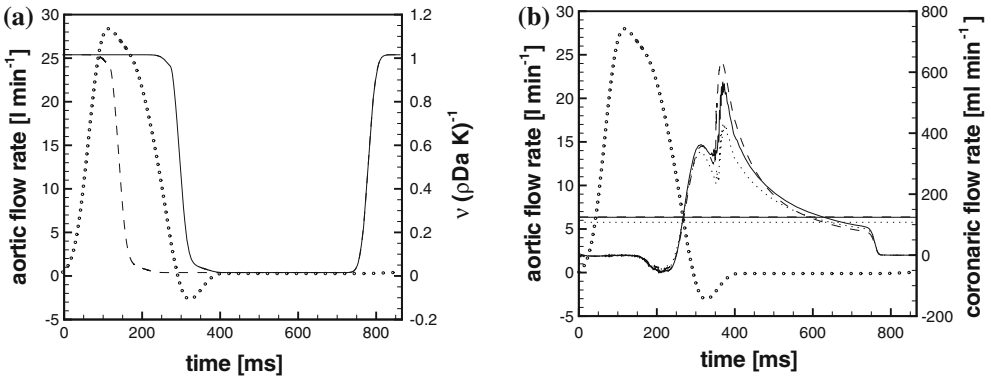

Fig. 15 **a** Forcing term $\mathbf{f}'$ (4) inside coronaries in function of time, *solid line* standard case, *dashed line* anticipated case. **b** time variation of the phase-averaged total coronaric flow rate for channels with $D_c = 3$ mm and anticipated forcing (lines as in Fig. 14)

flow after maximal vasodilatation in the presence of sinuses or pseudo-sinuses, that could indicate the presence of a more complex regulatory mechanism -not available for modeling- and a role of sinuses or pseudo-sinuses in modulating the coronary flow pattern.

4 Discussion

The present work studied the effects of the geometry of the aortic root on the pulsatile blood flow and on the coronary entry-flow, after the implant of a prosthetic bi-leaflet aortic heart valve. Although this study can be considered as a follow-up of de Tullio et al. [15], where all the validations of the numerical procedure and the basic flow analysis were shown, there are relevant novelties like the inclusion of the coronary arteries that, to the authors knowledge, was never considered before in such a complex configuration.

The modeling of the coronary flow turned out to be particularly challenging owing to the *pressure tissue effect* [26] that allows a relevant flow in the coronary network only during the diastole, when the ventricles are relaxed and extravascular compression of the coronary vessels is almost absent. The correct flow behavior was obtained by adding to the Navier-Stokes equations an extra forcing term (only inside the coronary channels) that modulates in time the porosity, and therefore mimics the resistance during flow perfusion into the coronary bed. We wish to point out that this method is very general since an adequate modulation of the forcing can reproduce, in principle, any flow rate behavior. On the other hand, due to the lack of the physical knowledge of an effective porosity measure, this forcing requires a preliminary tuning against a known flow that must be taken as reference case. In absence of adequate geometrical details of the complete network, we considered only the two main coronary vessels departing from two of the sinuses of Valsalva, truncating the complex branching structure of the vascular system. Therefore, the artificial outlet sections of the two coronary channels do not correspond to any physical interface. These outlet sections are maintained at the same left-ventricular pressure during the cardiac cycle. Such boundary conditions are limiting in that, in general, they do not accurately replicate vascular impedance of the downstream vasculature. One should consider the inertia of the fluid of all the neglected parts of the network, combined with the fact that the coronary arteries have a considerable degree of compliance. Based on an analogy between electrical and hydraulic nets, several models of the coronary circulation have been developed (see the work of [8,25,32] and references therein), including also autoregulation mechanisms which operate when the equilibrium of the biological system is disturbed, giving results in good agreement with the behavior of the natural system. Zero-dimensional and one-dimensional models cannot account for the fluid dynamics of the system in terms of local quantities, but they can provide the boundary conditions for the limited three-dimensional domain considered. Therefore, a coupling with the three-dimensional computational domain with one-dimensional or zero-dimensional models of the discarded network should be used (see [18,28] for a detailed description of the methods for prescribing such conditions in finite domains), in order to obtain a highly realistic flow rate and pressure fields.

A different approach is presented in this work. The inertial and capacitive effects do not occur in isolation but in combination with the ever-present resistance to flow due to viscous effects, depending on parameters that are difficult to estimate. As argued in details in Zamir [51], possibly the most important role which inertial

effects may play in the dynamics of the coronary circulation is that of acting as a balance for capacitive effects: this phenomenon points to the existence of an optimum condition of the system, in which coronary circulation very likely operates, that minimizes the effects of *reactance* (inertial and capacitive). Any disruption, due to vascular diseases, drugs or surgery, will move the system away from its optimal dynamics. Therefore we consider the total coronary flow behaving near the optimum conditions, dominated by resistive flow and with inertial and capacitive effects that balance each other. Even if there is no proof of evidence of this *ideal* condition, we considered this option physically valid for our purpose, that is the evaluation of the effect of the aortic root on the coronary-entry flow, while the coupling of our computational domain with zero-dimensional or one-dimensional models of the coronary system will be considered as a future improvement of the presented investigation. It is a first approximation, with just one parameter to be modeled (the porosity and hence the resistance to flow), that allowed us to avoid coupling techniques, since the porosity is controlled within the simulation for the points inside the coronaries. This choice is motivated by the fact that the physiological mean coronary flow is about 5% of the aortic flow [17]; therefore, we expect that the capacitive and inertial effects of the coronary network are negligible with respect to the complete system considered (aortic root and main coronary channels). Moreover, the effect of the coronary system on the main aortic flow is not relevant, as also indicated by the lumped model in Mantero et al. [32], where the addition of the coronary model does not modify or compromise the operation of the initial model of the cardiovascular system. At this level, the correctness of our model can be guided by a comparison of the results of the model in terms of flow rate with direct measurements available: The forcing was then tuned to reproduce a typical coronary flow rate extracted from echo-cardiographic imaging in a healthy young man. Maintaining the same forcing for all the geometries is physically equivalent to have always the same (time-variable) drag of the complex vascular network downstream of the coronaries, and this is a natural assumption since the coronary network is not modified by the surgery of the aortic root. Therefore, the results presented should be considered significant when compared for the different configurations, rather than considered as absolute results.

The first result is that the geometry of the aortic root affects only marginally the kinematic features of either the aortic and coronary flows, showing only minor changes in velocities in the different cases. This has been confirmed under different conditions, changing the coronary diameter, corresponding to different levels of vasodilatation due to rest or exercise. A result that is in agreement with the in vivo observations of De Paulis et al. [14].

Despite this, dynamical differences are noticeable. The maximum pressure levels, at the junctions between the coronary arteries and the aortic root, are significantly reduced in the geometry with three physiological sinuses with respect to a straight tube graft. These pressure differences are not negligible when reported in dimensional units as they can be of the order of 10 mmHg and they can significantly affect the aortic root pulse pressure (defined as the difference between systolic and diastolic blood pressure) that is of the order of 50 mmHg. It is known that chronically elevated distending pressures are responsible for the acceleration of age-associated increase of the aortic root diameter. The problem is further exacerbated in presence of a prosthetic aortic root, since a local pressure increase may support the development of post-procedural complications, like the bleeding of the coronary intersections with the graft and the pseudo-aneurysm formation [14]. In addition, it has recently been observed by Weltert et al. [48] that, even with an identical pressure level of the fluid, the structural stresses at the junction of the coronaries with the graft are lower (by $\sim 40\%$) in the case of an aortic root with a bulb (Fig. 4b) with respect to a straight pipe (Fig. 4c). We could then conjecture that a geometry like that of Fig. 4a, by combining a lower fluid pressure level with a decrease of the stresses from the structure side, could have beneficial consequences on the long-term survival of the patients.

A further result concerns the influence of the aortic root geometry on the dynamics of the valve. The overall behavior of the leaflets is similar in all the cases. There is, however, an important difference at the closure point when the leaflets hit the valve housing. It has been found that in correspondence of the natural aortic root, with three sinuses, the leaflets close with an angular velocity that is significantly smaller (up to 250%) than in the case of a straight cylindrical shape. This is a remarkable difference, since the violent deceleration of the leaflets at the valve closure causes haemolysis via the squashing of the blood cells, a phenomenon that requires the use of a continuous drug therapy to avoid the development of thrombus via platelet aggregation [19,21,30]. In addition, the collision between leaflets and valve housing is the cause of the noise produced by the mechanical valve closure and an impact at a reduced angular velocity is likely to generate less noise. The rhythmic sound of mechanical valves is such an annoying problem that a psychological evaluation of the patient is often part of the decision process about whether a biological or a mechanical valve implant should be preferred.

The theoretical predictions of this work are obtained in somehow idealized conditions. In particular, the flexibility of the valve holder, as well as that of aortic walls is not considered, missing information about

the variations introduced by compliant walls to these results. Moreover, since the flow is incompressible, considering rigid walls means that wave phenomena are not included. Therefore, care must be exercised in extrapolating the results to in vivo behavior of mechanical heart valves, while a clinical confirmation of these results would have an immediate beneficial impact on the quality of the surgical therapy.

Acknowledgments Several large-scale simulations in this paper were possible thank to the support and computer facilities of CASPUR (Consorzio interuniversitario per le Applicazioni di Supercalcolo Per Università e Ricerca) through contract STD09–331. Drs. F. Massaioli and G. Amati are gratefully acknowledged for their continuous technical support. The financial support of CEMeC (Centro d'Eccellenza di Meccanica Computazionale) of Politecnico di Bari is also gratefully acknowledged.

References

1. Apel, J., Reinhard, P., Klaus, S., Siess, T., Reul, H.: Assessment of hemolysis related quantities in a microaxial blood pump by computational fluid dynamics. Artif. Organs **25**, 341–347 (2001)
2. Attinger, E.O.: Pulsatile Flow. McGraw-Hill, New York (1963)
3. Bentall, H., De Bono, A.: A technique for complete replacement of the ascending aorta. Thorax **23**, 338–339 (1968)
4. Borazjani, I., Ge, L., Dasi, P.L., Sotiropoulos, F., Yoganathan, A.P.: Fluid-structure interaction in bi-leaflet mechanical heart valves. In 2nd Frontier in Biomedical Devices Conference, California, USA, BioMed 2007-3807, 7–8 June 2007
5. Borazjani, I., Ge, L., Sotiropoulos, F.: High-resolution fluidstructure interaction simulations of flow through a bi-leaflet mechanical heart valve in an anatomic aorta. Ann. Biomed. Eng. **38**, 326–344 (2010)
6. Choi, C.R., Kim, C.N.: Numerical analysis on the hemodynamics and leaflet dynamics in a bileaflet mechanical heart valve using a fluid-structure interaction method. ASAIO J. **55**, 428–437 (2009)
7. Cochran, R.P., Kunzelman, K.S., Eddy, A.C., Hofer, B.O., Verrier, E.D.: Modified conduit preparation creates a pseudosinus in an aortic valvesparing procedure for aneurysm of the ascending aorta. J. Thorac. Cardiovasc. Surg. **109**, 1049–1058 (1995)
8. Cox, L.G.E., Loerakker, S., Rutten, M.C.M., de Mol, B.A.J.M., van de Vosse, F.N.: A mathematical model to evaluate control strategies for mechanical circulatory support. Artif. Organs **33**, 593–603 (2009)
9. Cristallo, A., Verzicco, R.: Combined immersed boundary/large-eddy-simulations of incompressible three dimensional complex flows. Flow Turbulence Combustion **77**, 3–26 (2006)
10. Dasi, L.P., Ge, L., Simon, H.A., Sotiropoulos, F.P., Yoganathan, A.: Vorticity dynamics of a bileaflet mechanical heart valve in an axisymmetric aorta. Phys. Fluids **19**, 1–17 (2007)
11. David, T.E., Armstrong, S., Ivanov, J., Feindel, C.M., Omran, A., Webb, G.: Results of aortic valve-sparing operations. J. Thorac. Cardiovasc. Surg. **122**, 39–46 (2001)
12. David, T.E., Feindel, C.M.: An aortic valve-sparing operation for patients with aortic incompetence and aneurysm of the ascending aorta. J. Thorac. Cardiovasc. Surg. **103**, 617–622 (1992)
13. De Paulis, R., De Matteis, G.M., Nardi, P., Scaffa, R., Colella, D.F.F., Chiarello, L.: A new aortic Dacron conduit for surgical treatment of aortic root pathology. Thorax **1**, 457–463 (2000)
14. De Paulis, R., Tomai, F., Bertoldo, F., Ghini, A.S., Scaffa, R., Nardi, P., Chiarello, L.: Coronary flow characteristics after a Bentall procedure with or without sinuses of Valsalva. Eur. J. Cardio-Thorac. Surg. **26**, 66–72 (2004)
15. de Tullio, M.D., Cristallo, A., Balaras, E., Verzicco, R.: Direct numerical simulation of the pulsatile flow through an aortic bileaflet mechanical heart valve. J. Fluid Mech. **622**, 259–290 (2009)
16. Fadlun, E.A., Verzicco, R., Orlandi, P., Mohd-Yosuf, J.: Combined immersed-boundary finite-difference methods for three-dimensional complex flow simulations. J. Comput. Phys. **161**, 35 (2000)
17. Folkow, B., Neil, E.: Circulation. Oxford University Press, New York (1971)
18. Formaggia, L., Veneziani, A., Vergara, C.: A new approach to numerical solution of defective boundary vaule problems in incompressible fluid dynamics. SIAM J. Numer. Anal. **46**, 2769–2794 (2008)
19. Giersiepen, M., Wurzinger, L.J., Opitz, R., Reul, H.: Estimation of shear stress related blood damage in heart valve prosteses: in vitro comparison of 25 aortic valves. Int. J. Artif. Organs **13**, 300–306 (1990)
20. Grigioni, M., Daniele, C., Del Gaudio, C., Morbiducci, U., Balducci, A., D'avenio, G., Barbaro, V.: Aortic bileaflet valve in a realistic model of aortic root. ASAIO J. **51**, 176–183 (2005)
21. Grigioni, M., Morbiducci, U., D'Avenio, G., Di Benedetto, G., Del Gaudio, C.: A novel formulation for blood trauma prediction by a modified power-law mathematical model. Biomech. Model Mechanobiol. **4**, 249–260 (2005)
22. Guivier-Curien, C., Deplano, V., Bertrand, E.: Validation of a numerical 3-D fluidstructure interaction model for a prosthetic valve based on experimental PIV measurements. Med. Eng. Phys. **31**, 986–993 (2009)
23. Horseld, K., Woldenberg, M.J.: Diameters and cross-sectional areas of branches in the human pulmonary arterial tree. Anat. Rec. **223**, 245–251 (1989)
24. Iaccarino, G., Verzicco, R.: Immersed boundary technique for turbulent flow simulations. Appl. Mech. Rev. **56**, 331 (2003)
25. Jacobs, J., Algranati, D., Lanir, Y.: Lumped flow modeling in dynamically loaded coronary vessels. J. Biomech. Eng. **130** (2008)
26. Kajiya, F., Matsuoka, S., Ogasawara, Y., Hiramatsu, O., Kanazawa, S., Wada, Y., Tadaoka, S., Tsujioka, K., Fujiwara, T., Zamir, M.: Velocity profiles and phasic flow patterns in the non-stenotic human left anterior descending coronary artery during cardiac surgery. Cardiovasc. Res. **27**, 845–850 (1993)

27. Karck, M., Amd Kallenbach, K., Hagl, C., Rhein, C., Leyh, R., Haverich, A.: Aortic root surgery in marfan syndrome: Comparison of aortic valve-sparing reimplantation versus composite grafting. J. Thorac. Cardiovasc. Surg. **127**, 391–398 (2004)
28. Kim, H.J., Figueroa, C.A., Hughes, T.J.R., Jansen, K.E., Taylor, C.A.: Augmented Lagrangian method for constraining the shape of velocity profiles at outlet boundaries for three-dimensional finite element simulations of blood flow. Comput. Methods Appl. Mech. Eng. **198**, 3551–3556 (2009)
29. Kleine, P., Scherer, M., Abdel-Rahman, U., Klesius, A.A, Ackermann, H., Moritz, A.: Effect of mechanical aortic valve orientation on coronary artery flow: Comparison of tilting disc versus bileaflet prostheses in pigs. Surg. Acquir. Cardiovasc. Dis. **124**, 925–932 (2002)
30. Kuypers, F.A.: Red cell membrane damage. J. Heart Valve Dis. **7**, 387–395 (1998)
31. Malvern, L.E.: Introduction to the Mechanics of a Continuous Medium. Prentice Hall Inc, Englewood Cliffs (1977)
32. Mantero, S., Pietrabissa, R., Fumero, R.: The coronary bed and its role in the cardiovascular system: a review and an introductory single-branch model. J. Biomed. Eng. **14**, 109–115 (1992)
33. Mayrovitz, H.N., Roy, J.: Microvascular blood flow: evidence indicating a cubic dependence on arteriolar diameter. Am. J. Physiol. Heart Circ. Physiol. **245**, H1031–H1038 (1983)
34. Morbiducci, U., Ponzini, R., Nobili, M., Massai, D., Montevecchi, F.M., Bluestein, D., Redaelli, A.: Blood damage safety of prosthetic heart valves. Shear-induced platelet activation and local flow dynamics: A fluidstructure interaction approach. J. Biomech. **42**, 1952–1960 (2009)
35. Nichols, W.W., O'Rourke, M.F.: Mc Donald's blood flow in arteries. Lea & Febiger, Philadelphia, PA (1990)
36. Nobili, M., Morbiducci, U., Ponzini, R., Del Gaudio, C., Balducci, A., Grigioni, M., Montevecchi, F.M., Redaelli, A.: Numerical simulation of the dynamics of a bileaflet prosthetic heart valve using a fluid-structure interaction approach. J. Biomech. **41**, 2539–2550 (2008)
37. Popov, E.P.: Mechanics of materials. 2nd edn. Prentice Hall Inc, Englewood Cliffs (1976)
38. Reul, H., Vahlbruch, A., Giersiepen, M., Schmitz-Rode, T., Hirtz, V., Effert, S.: The geometry of the aortic root in health, at valve disease and after valve replacement. J. Biomech. **23**, 181–191 (1990)
39. Rodbard, S.: Vascular caliber. Cardiology **60**, 4–49 (1975)
40. Romano, G.P.: Deliverable d24-study case report n 2 pulse duplicator with aortic root model from rwth aachen smart-piv ist-2002-37548 european project. (2008) http://www.smart-piv.com
41. Sarsam, M.A., Yacoub, M.: Remodeling of the aortic valve anulus. J. Thorac. Cardiovasc. Surg. **105**, 435–438 (1993)
42. Sorin-Group. Sorin Biomedica. (2006) http://www.sorinbiomedica.com
43. Sotiropoulos, F., Borazjani, I.: A review of the state-of-the-art numerical methods for simulating flow through mechanical heart valves. Med. Biol. Eng. Comput. **47**, 245–256 (2009)
44. Swartzrauber, P.N.: A direct method for the discrete solution of separable elliptic equations. SIAM J. Numer. Anal. **11**, 1136–1150 (1974)
45. Verhey, J.F, Bara, C.: Influence on fluid dynamics of coronary artery outlet angle variation in artificial aortic root prosthesis. Biomed. Eng. OnLine **7**, 9+ (2008)
46. Verzicco, R., Orlandi, P.: A finite difference scheme for threedimensional incompressible flows in cylindrical coordinates. Journal of Computational Physics **123**, 402–413 (1996)
47. Wellnhofer, E., Goubergrits, L., Kertzscher, U., Affeld, K.: In–vivo coronary profiling based on biplane angiograms: influence of geometric simplifications on the threedimensional reconstruction and wall shear stress calculation vascular caliber. Biomedical Engineering Online **5**, 39 (2006)
48. Weltert, L., De Paulis, R., Scaffa, R., Maselli, D., Bellisario, A., D'Alessandro, S.: Re-creation of a sinuslike graft expansion in Bentall procedure reduces stress at the coronary button anastomoses: A finite element study. J. Thorac. Cardiovasc. Surg. **137**, 1082–1087 (2009)
49. Yacoub, M.H.: Valve-Conserving Operation for Aortic Root Aneurysm or Dissection, pp. 57–67. WB Saunders, Philadelphia (1996)
50. Yang, J., Preidikman, S., Balaras, E.: A strongly—coupled embedded boundary method for fluid–structure interaction of elastically mounted rigid bodies. J. Fluids Struct. **182**, 167–182 (2008)
51. Zamir, M.: The Physics of Coronary Blood Flow. Springer (2005)
52. Zamir, M., Chee, H.: Branching characteristics of human coronary arteries. Can. J. Physiol. Pharmacol. **64**, 661–668 (1986)